SPACE SCIENCES

Absence of a long-lived lunar paleomagnetosphere

John A. Tarduno[1,2]*, Rory D. Cottrell[1], Kristin Lawrence[3†], Richard K. Bono[4], Wentao Huang[1], Catherine L. Johnson[3,5], Eric G. Blackman[2], Aleksey V. Smirnov[6,7], Miki Nakajima[1,2], Clive R. Neal[8], Tinghong Zhou[1], Mauricio Ibanez-Mejia[9], Hirokuni Oda[10], Ben Crummins[1]

Determining the presence or absence of a past long-lived lunar magnetic field is crucial for understanding how the Moon's interior and surface evolved. Here, we show that Apollo impact glass associated with a young 2 million–year–old crater records a strong Earth-like magnetization, providing evidence that impacts can impart intense signals to samples recovered from the Moon and other planetary bodies. Moreover, we show that silicate crystals bearing magnetic inclusions from Apollo samples formed at ~3.9, 3.6, 3.3, and 3.2 billion years ago are capable of recording strong core dynamo–like fields but do not. Together, these data indicate that the Moon did not have a long-lived core dynamo. As a result, the Moon was not sheltered by a sustained paleomagnetosphere, and the lunar regolith should hold buried ^{3}He, water, and other volatile resources acquired from solar winds and Earth's magnetosphere over some 4 billion years.

INTRODUCTION

Three outstanding questions center on the Moon's past magnetism. The first asks whether the lunar core could have generated a long-lived dynamo producing a strong surface field (*1*–*2*). The second asks whether the associated magnetosphere contributed to the protection of Earth's atmosphere from erosion by early solar winds (*3*–*4*). The third asks whether a lunar paleomagnetosphere blocked ion transport from the solar wind and Earth, ultimately limiting these as long-term sources of volatiles (*5*) in the lunar regolith. These questions further stem from the surprising discovery of magnetism in some of the lunar rocks returned from the Apollo missions.

Paleointensity estimates published in the 1970s and '80s were interpreted as evidence for a global lunar magnetic field between 3.9 and 3.6 billion years (Ga) ago as strong as or stronger than that of Earth today [e.g., (*1*)]. The difficulties in generating such high field strengths in the small lunar core were recognized in these works. Further caveats about the early data stem from the nonideal nature of magnetic carriers in lunar samples and techniques used to retrieve paleofield strength estimates. Many lunar samples show nonideal multidomain-like magnetic characteristics. Analysis methods have commonly relied on the application of laboratory magnetic fields rather than thermal treatments that duplicate the thermoremanent magnetization (TRM) process (*6*), which might have imparted primary magnetizations to lunar rocks. Moreover, many Apollo samples are the products of impacts (glasses and breccias), and concerns were raised that magnetizations could be imparted by shock (*7*). Satellite data show very weak crustal magnetic fields over much of the lunar crust [e.g., figure 1 of (*8*)]. The low strength and deep source depths are interpreted to record magnetizations acquired during crustal cooling before 4.4 Ga ago (*8*). Relatively stronger anomalies around part of the South Pole–Aitken basin could reflect impact-delivered iron during this time (*8*). However, other magnetic anomalies do not form a clear pattern in space or time. In particular, vast areas of mare basalts formed during the proposed high–magnetic field epoch lack magnetic signatures (fig. S1).

The paradox of lunar magnetizations lay fallow for 25 years until it was revisited by Lawrence *et al.* (*9*). Thellier double-heating experiments that replicate the TRM process yielded results that questioned a long-lived lunar dynamo, but one of the samples analyzed was subsequently measured by another group using nonthermal methods, and the data were interpreted as further evidence for an ancient dynamo (*10*). Moreover, the age of a strong dynamo field was extended beyond that originally proposed (*1*), to older ages (*10*), and then with additional nonthermal measurements to younger ages, the latter giving rise to the concept of a "late lunar dynamo" at 3.56 Ga (*11*). This prompted new models of potential lunar dynamo generation (*12*–*13*), but none can successfully predict the high sustained Earth-like field values (*2*). The conundrum has only deepened with the report of a ~1.5-Ga-old magnetization using Thellier thermal analysis from a lunar impact breccia and its interpretation as a record of an even later core dynamo field (*14*).

Against this background of sample data that seem to support a long-lived lunar dynamo [e.g., (*15*)], it is important to recognize that analyses before and since the 2008 Lawrence *et al.* study (*9*) have generated data that might indicate essentially null field values and the absence of a lunar dynamo (see Materials and Methods). Thus, the currently accepted concept of a long-lived lunar dynamo extending from ~4.2 to ~1.5 Ga relies not only on a choice of data that appear to record strong fields but also on two key corollaries that state the following: (i) These fields cannot be produced by any process other than a core dynamo, and (ii) data recording null fields are not accurate because the samples cannot record strong fields.

Recently, a Thellier analysis has been reported on a 1-Ga-old Apollo sample and interpreted as representing the cessation of the lunar dynamo (*16*). Here, we first study an Apollo glass sample linked to a 2–million year (Ma)–old impact that, following this timeline, is predicted to have no remanent magnetization imparted

[1]Department of Earth and Environmental Sciences, University of Rochester, Rochester, NY 14627, USA. [2]Department of Physics and Astronomy, University of Rochester, Rochester, NY 14627, USA. [3]Planetary Science Institute, Tucson, AZ 85719-2395, USA. [4]Geomagnetism Laboratory, University of Liverpool, Liverpool L69 3GP, UK. [5]Department of Earth, Ocean and Atmospheric Sciences, University of British Columbia, Vancouver, BC V6T 1Z4, Canada. [6]Department of Geological and Mining Engineering and Sciences, Michigan Technological University, Houghton, MI 49931, USA. [7]Physics Department, Michigan Technological University, Houghton, MI 49931, USA. [8]Department of Civil and Environmental Engineering and Earth Sciences, University of Notre Dame, Notre Dame, IN 46556, USA. [9]Department of Geosciences, University of Arizona, Tucson, AZ 85721, USA. [10]Research Institute of Geology and Geoinformation, Geological Survey of Japan, National Institute of Advanced Industrial Science and Technology (AIST), Tsukuba 305-8567, Japan.
*Corresponding author. Email: john.tarduno@rochester.edu
†Work done while affiliated with PSI.

from a dynamo. We instead find a strong Earth-like magnetization and show that its origin is related to the impact that formed the sample. This discovery provides evidence for a mechanism that discounts corollary (i) with implications more broadly for planetary magnetizations. This leads us to an examination of corollary (ii) through the analysis of five additional lunar samples with ages spanning the putative lunar high-field epoch (*1*) and its extension to the late lunar dynamo. We find that these samples are capable of recording strong dynamo-like fields but instead have negligible remanent magnetizations, compatible with a null lunar field and discounting corollary (ii).

These findings allow us to address the three salient questions about the lunar magnetizations. As we will show, our new data indicate that the Moon did not have a long-lasting core dynamo. Thus, a sustained lunar paleomagnetosphere was not present, which might have helped protect Earth's atmosphere from solar winds. Instead, the lunar regolith should record ion transport from the solar wind and Earth's magnetosphere over some 4 Ga.

RESULTS

We start by analyzing lunar sample 64455 (fig. S2), a ~5 cm–by–3 cm ovoid-shaped basaltic impact melt linked to the ~680-m-diameter South Ray crater (*17*–*18*). The sample was collected ~4380 m from the center of the crater and has a thick glass rim having a delicate, smooth exterior that almost completely covers the rock (*17*). It has cosmogenic exposure ages of 2 Ma [see Materials and Methods and (*19*)], and the distribution of micrometeorite "zap" pits suggests that it has maintained its orientation on the lunar surface since it landed. On the basis of the physical nature of the sample, the glass composition, the site geology, and the consistency of exposure ages from 22 associated Apollo samples, the glass formation age is thought to be 2 Ma, coinciding with the impact that formed South Ray crater (see Materials and Methods). We focus our analyses on the glass (Fig. 1A); light microscopy reveals that glass subsamples contain spherical metallic inclusions that are <1 to 5 μm in size but that are sometimes as large as 100 μm in diameter (Fig. 1B) (see Materials and Methods). Magnetic hysteresis measurements (see Materials and Methods) show thin curves indicative of a dominance of low coercivities typical of lunar samples (Fig. 1C). A clear wasp-waisted (*20*) nature to the curves may suggest the presence of ultrafine superparamagnetic (SP) grains. Another distinct feature is the very high ratio of coercivity of remanence (B_{cr}) to coercivity (B_c) (B_{cr}/B_c = 16.6; table S1), different from typical terrestrial carriers but characteristic of lunar samples (fig. S3). First-order reversal curve (FORC) diagrams (see Materials and Methods) show a central peak that is slightly asymmetric with a downward trend with increasing estimated coercivity that may be a sign of minor interactions (Fig. 1, C and D).

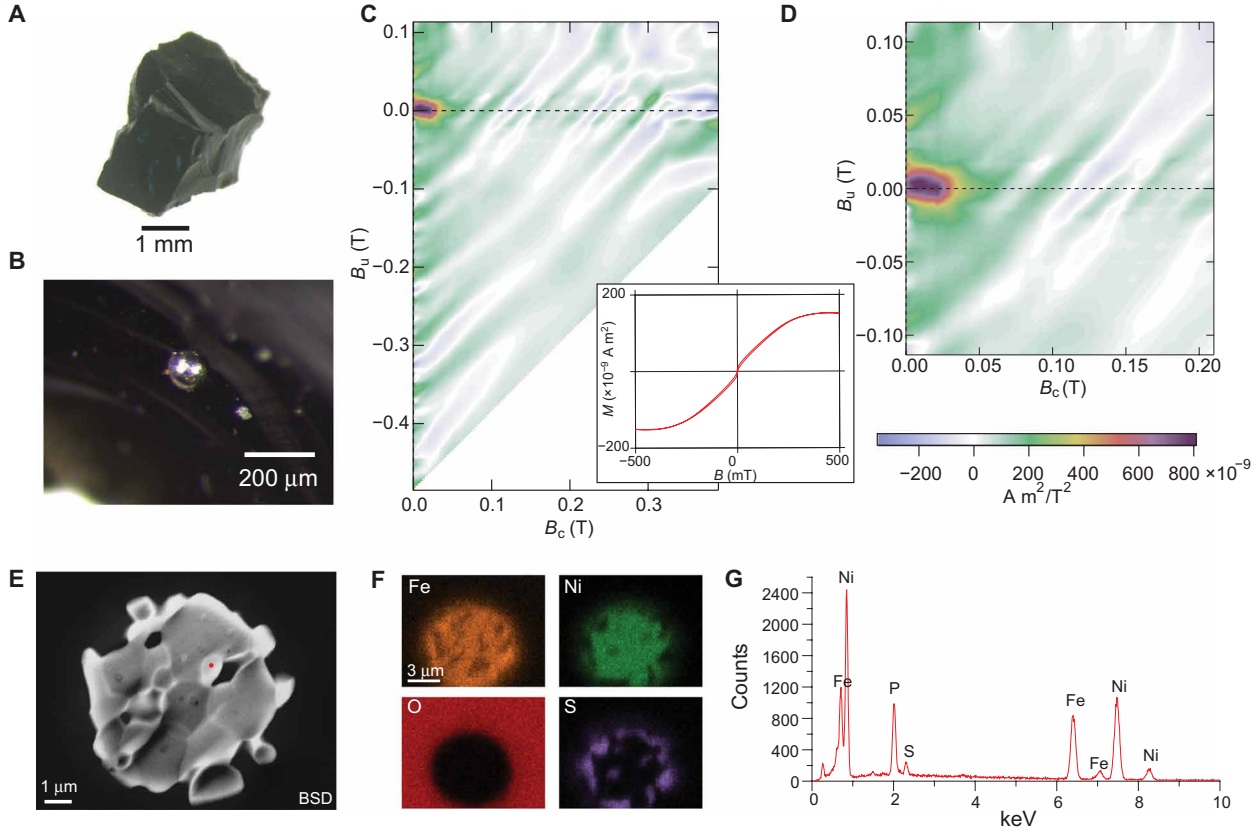

Fig. 1. Light and electron microscope imaging and rock magnetic analyses of Apollo sample 64455. (**A**) Glass from Apollo sample 64455. (**B**) Light microscope image of typical largest metallic spheres observed. Smaller sphere in background. (**C**) FORCs for subsample 64455-ss55. Saturating field, 1 T; number of FORCs, 156; field increment, 6 mT. Smoothing criteria (see Materials and Methods): Sc0 = 7, Scb = 5, Sc1 = Sb1 = 8, and $\lambda_h = \lambda_v = 0.20$. The inset shows individual magnetic hysteresis loop corrected for paramagnetic slope. (**D**) Detail of central portion of (C). (**E** to **G**) SEM data for 64455 glass subsample, inclusion (B). (E) Backscatter detector image, 20-keV beam strength. (F) Energy-dispersive spectroscopy (EDS) maps. (G) Spectral analyses (EDS) of spots labeled in (E). See table S2 for compositional estimates from the EDS data.

There is no evidence for a very high coercivity signal; overall, the individual hysteresis curves and FORCs suggest pseudosingle domain–like grains mixed with SP particles. Scanning electron microscopy (SEM) and energy dispersive analyses of unheated subsamples (see Materials and Methods) reveal that magnetic particles are concentrated in the spheres, which have a diversity of internal structures and distributions of Fe, Ni, and S (Fig. 1, E to G, and figs. S4 to S10). Fe/Ni estimates (table S2), together with the magnetic coercivities and the glass setting, indicate that body-centered martensitic and face-centered taenite compositions and structures have been quenched in the inclusions within the glass. Ni contents are higher than some other lunar samples and may indicate the incorporation of impactor material into the glass.

Thermally induced alteration is a well-known problem in paleointensity analyses of lunar samples. However, prior concerns have focused on chemical alteration and not on attendant changes in magnetic structure [e.g., (*6*)]. Here, we use rapid, brief heating using CO_2 laser methods to limit both effects (see Materials and Methods). Total TRM (TTRM) experiments, whereby the natural remanence is compared to that imparted at a single temperature, can be used to yield a first-order assessment of paleointensity (see Materials and Methods). We select a temperature (590°C) that covers much of the predicted unblocking temperature spectrum of potential magnetic carriers. We first apply thermal treatment to a test specimen (see Materials and Methods). A comparison of magnetic hysteresis data before and after heating shows no evidence for changes in domain state, and we conclude that the rapid and brief heating is insufficient to create or destroy magnetic minerals (fig. S11). TTRM demagnetization data show the inability of one subsample to accurately record the field at high unblocking temperatures, and minor structural changes with heating are hinted at by the lack of perfect replication of the natural remanent magnetization (NRM) and TTRM demagnetization curves (fig. S12, A to C). Nevertheless, these changes appear to be minor because the NRM versus TTRM loss data over a temperature segment with a characteristic component of magnetization from two subsamples yield replicable paleointensity estimates of 12.2 ± 0.7 and 11.6 ± 4 μT (Fig. 2A and fig. S12).

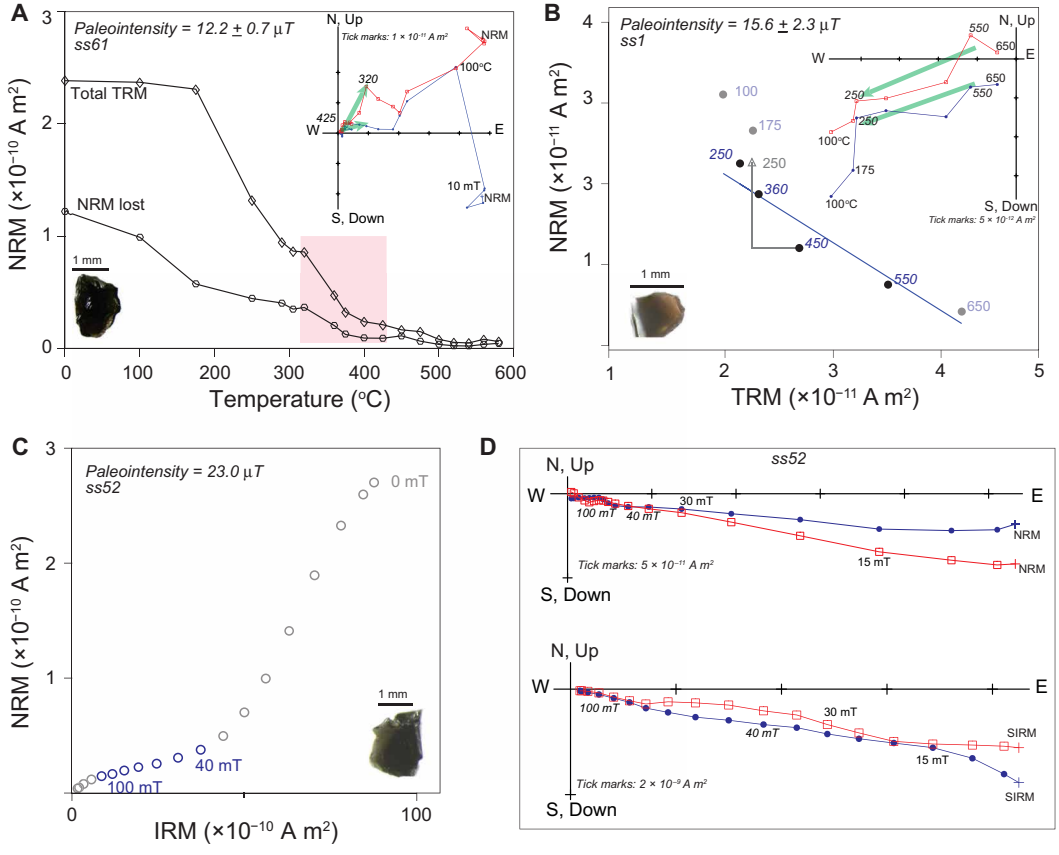

Fig. 2. Paleointensity analyses on Apollo 64455 glass. Subsamples measured are shown as inset in (A to C). (**A**) TTRM experiment. Plot of the decay of NRM and laboratory-induced TTRM with temperature. The pink shaded region represents steps used to determine the paleointensity value. The inset shows the orthogonal vector plot of NRM demagnetization. A three-point sliding window average was used to reduce noise in the remanence signal and determine the characteristic remanent magnetization (ChRM) using principal components analysis (green arrows). Red, inclination (vertical) component; blue, declination (horizontal) component. (**B**) Thellier-Coe paleointensity experiment. The loss of NRM is plotted against the acquisition of a laboratory-induced TRM (circles) and (pTRM) check (triangle). Black circles/blue labels identify data used to fit paleointensity. The inset shows orthogonal vector plot of field-off steps. Conventions as in (A). Labels in italics identify temperature range used in paleointensity fit. (**C** and **D**) REM′ paleointensity determination. (C) The loss of NRM plotted against loss of IRM. (D) Orthogonal vector plot of AF demagnetization of NRM (top) and 3-T saturating IRM (bottom); conventions as in (A). The slope of the line in (C) that matches the AF range, where the ChRM is defined in the NRM orthogonal vector plot [40 to 100 mT in (D)], is related to the paleofield strength by a calibration factor (see Materials and Methods).

Some subsamples chosen for the more robust double-heating Thellier-Coe paleointensity analyses (see Materials and Methods) showed evidence for multiple components and/or changing directions after field-off thermal treatments. Others show evidence for thermally induced chemical or structural changes and/or nonideal recording behavior, but three subsamples (12%) pass partial TRM (pTRM) checks and yield paleointensity values of 15.6 ± 2.3, 18.1 ± 3.1, and 23.5 ± 4.7 μT (Fig. 2B, fig. S13, and table S3). We also applied the ratio of equivalent magnetizations (REM′) nonheating paleointensity method (Fig. 2, C and D, and fig. S14), applying a saturation isothermal remanent magnetization (SIRM), and demagnetizations using alternating fields (AFs) with smoothing to address gyroremanent magnetization (GRM) effects; ultimately, this method relies on the use of calibration data (see Materials and Methods). This approach yields values ranging from ~23 to ~39 μT, not considering uncertainties in data fits or calibrations, or ~10 to ~89 μT, considering these uncertainties (see Materials and Methods and table S4).

The mean paleointensity estimates for the 64455 glass based on thermal and nonthermal methods are fascinating because fields this strong have been interpreted as evidence for a dynamo in samples billions of years old (*1*). The linkage of 64455 glass to South Ray crater suggests an age that is millions, not billions, of years old, and at this time, the Moon's interior thermal state would have been indistinguishable from that of today, incapable of sustaining a core dynamo. The lack of a dominant soft coercivity component indicates that spacecraft contamination is unlikely (*21*). Another possibility is the cooling in a local crustal magnetic field, but this is effectively discounted by the small magnetic fields of 112 ± 5 nT measured by Apollo 16 astronauts (*22*) and recent satellite measurements (*23*) that indicate surface fields orders of magnitude smaller than those needed to explain the 64455 paleointensity data.

A remaining possibility is a field imparted by the formation of the South Ray crater. Impacts can result in magnetizing fields through compression of the solar wind (*24*–*25*) or through charge separation (*26*); only the latter is relevant to magnetizations near the impact site and thus is considered here (see Materials and Methods). Experiments and detailed simulations (*26*) support generation of a field B at radius r for small impactors of radius R ($0.1 \leq R \leq 3$ km) following

$$B \sim 8.3 \times 10^{-4} (r/50R)^{-2} (R/1\,\mathrm{km}) (v/20\,\mathrm{km\,s^{-1}})^{3.6} \quad (1)$$

where v is the impactor velocity and B is in tesla. For larger impacts ($3 \leq R \leq 20$ km), the simulations using impactor velocities of 20 km s^{-1} support a relationship of

$$B \sim 7.2 \times 10^{-5} (R/1\mathrm{km}) + 2.23 \times 10^{-3} \quad (2)$$

where B is evaluated at $r = 50R$. From numerical simulations, Crawford (*26*) concluded that the magnetic anomalies of the lunar Crisium, Nectaris, Serenitatis, Humboldtianum, and Mendel-Rydberg basins could be accounted for by the charge separation–generated magnetizations associated with 20-km-radius impactors. Higher-velocity impactors such as comets can generate even larger fields (*27*). However, the charge-separation mechanism is expected to depend on numerous factors including velocity, the impactor composition, and impact angle, such that all impacts might not necessarily generate high fields. This is consistent with lunar observations where magnetic anomalies are associated with some large craters and not with others.

We model the impact using the hydrocode iSALE2D (see Materials and Methods), the findings of which suggest that an impactor 20 to 22 m in diameter can form the South Ray crater (fig. S15). Extrapolation of Eq. 1 to this size of impactor yields fields of ~18 to 24 μT at the edge of the crater, remarkably similar to the 64455 glass paleointensity (e.g., 19.1 ± 3.6 μT, mean value derived from Thellier analyses). This, in turn, implies that the magnetic minerals in the 64455 glass passed through their blocking temperatures during flight, consistent with the changing magnetization directions observed from some specimens during demagnetization. We note that prior paleomagnetic analysis of another young lunar glass, less than a few million years old and recovered from a 3-m crater, yielded data defining a nonzero NRM/TRM slope and a nominal field value of 2.5 μT (*28*). While that study did not use pTRM checks, the results nevertheless further suggest that ionization from small impacts can generate substantial magnetic fields.

Thus, fields generated by the impact itself are consistent with the high paleointensity values from the 64455 glass. The young lunar surface is a far better environment for recording and preserving impact magnetizations as compared to Earth (see Materials and Methods) because of the lack of a background dynamo field. Our results indicate, more generally, that magnetizations of other planetary bodies can be imparted by impacts, but our findings also have specific and profound implications for the Moon because the 64455 Apollo impact glass specimens have paleofield strengths that are comparable to those of the prior 4.2 Ga of the nominal lunar paleointensity record. There are more than a million known craters on the Moon similar to or larger than the size of South Ray crater (i.e., ≥1 km) and many thousands created by much larger impactors that would generate orders of magnitude stronger fields (see Materials and Methods). The Apollo lunar samples recording strong paleofields highlighted in prior works, therefore, may record external fields produced by impacts rather than an ancient core dynamo.

This finding provides motivation to revisit corollary (ii), which claims that prior measurements of null lunar fields from Apollo samples are inaccurate. Here, we apply the single silicate crystal paleointensity technique that strives to isolate samples with better magnetic properties than bulk samples by eliminating large multidomain grains [see Materials and Methods and (*29*)]. We select 13 crystals [e.g., Fig. 3 (A and G)] ~0.5 mm in size (range of 0.3 to 1.1 mm) from five basalt samples from the Apollo 17, 14, and 12 missions with ages of ~3.9 Ga (sample 14053), 3.6 Ga (sample 71055), 3.3 Ga (samples 12021 and 12040), and 3.2 Ga (sample 12053) (see Materials and Methods). These crystals are plagioclase or pyroxene; in a few cases (i.e., 14053 and 12021), plagioclase and pyroxene could not be completely separated, and the specimen investigated consists of both minerals. The magnetic mineralogy of lunar bulk rock basalts is mainly native iron together with minor Ni [<5 weight % (wt %)] or cobalt (<1 wt %) (*30*) and a kamacite body-centered structure. However, unlike the crystallization of typical magnetic phenocrysts in terrestrial basalts, this native iron and ilmenite form from the reduction of a parent ulvöspinel (*30*).

Clear evidence for magnetic grains that carry laboratory remanences is seen in magnetic hysteresis data (fig. S16) of both unheated plagioclase and pyroxene. SEM analyses (see Materials and Methods)

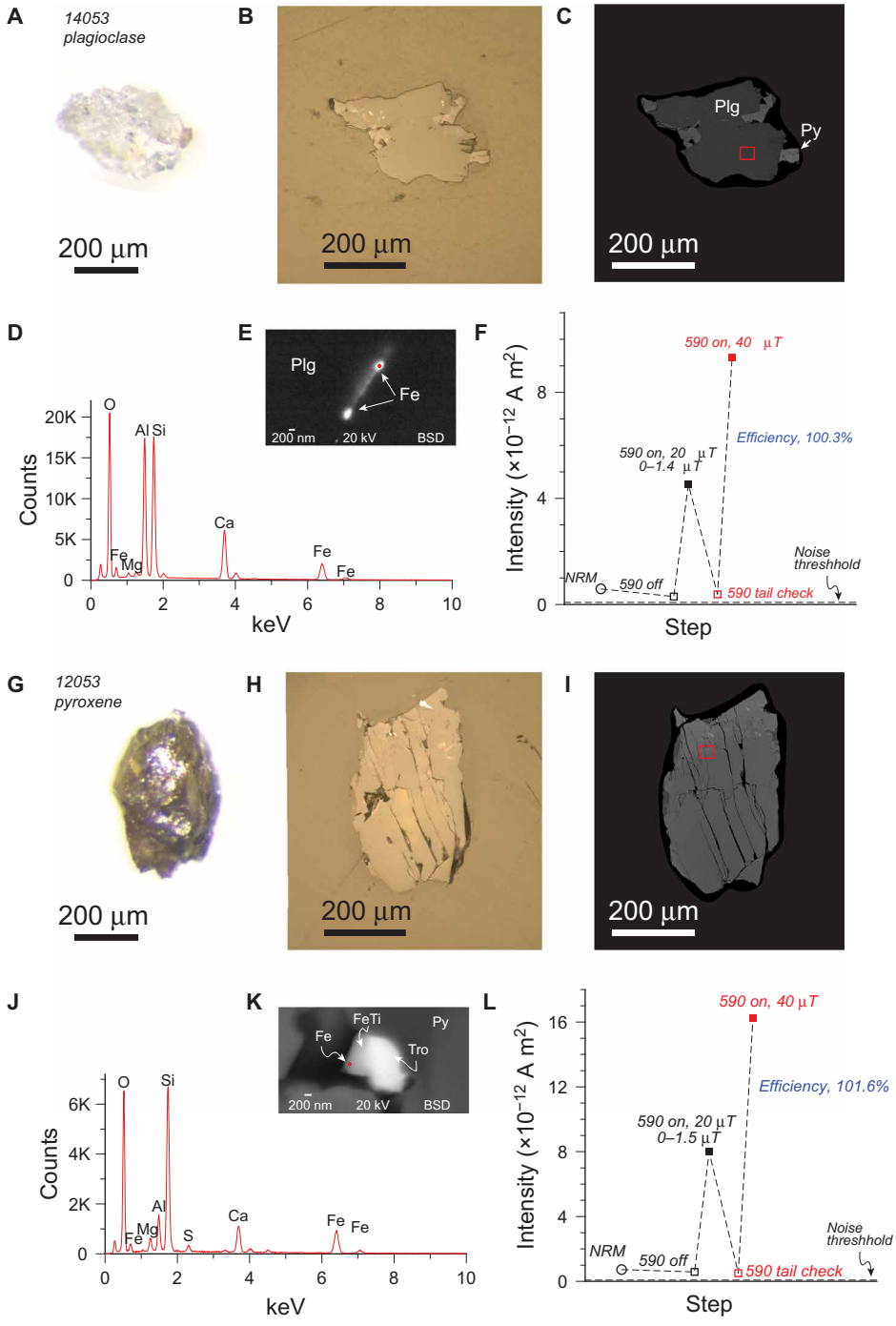

Fig. 3. Silicate crystals and TRM experiments. (**A** to **F**) Apollo sample 14053 (~3.9 Ga). (A) Transmission light microscopy photo. (B) Reflected light image of polished crystal. (C) SEM backscatter image. Plg, plagioclase; Py, pyroxene. The red box shows analysis area (D and E). (D) Elemental spectra [(red dot in (E)]. (E) SEM backscatter image of analysis area. (F) TRM experiment on grain imaged in (A to E). Intensity versus experimental step. Noise threshold is sensing limit of ultrasensitive superconducting quantum interference device (SQUID) magnetometer. Field value shown is nominal paleointensity range (see text). Efficiency is calculated from field-on values after applied fields of 20 and 40 µT. (**G** to **L**) Apollo sample 12053 (~3.2 Ga). (G) Transmission light microscopy photo. (H) Reflected light image of polished crystal. (I) SEM backscatter image. The red box shows analysis area (J and K). (J) Elemental spectra [red dot in (K)]. (K) SEM backscatter image of analysis area with phases identified. Tro, troilite. S in spectra is interpreted as contamination from nearby troilite. (L) TRM experiment on grain imaged in (G to K); plot follows conventions in (F).

of the exact grains used in paleointensity analyses described below show clear evidence for native iron particles [e.g., Fig. 3 (B to E)] with a range of submicrometer grain sizes (figs. S17 to S19). The iron grains documented in these SEM observations likely represent the large end of a spectrum that extends to even smaller sizes. Sometimes, iron particles are found in association with a FeTi phase and/or troilite [e.g., Fig. 3 (H to K)]. Magnetic phases other than iron are generally subordinate, except in Apollo 71055, where the

magnetic mineralogy contains more common FeCr phases and troilite. In this case, the iron is found as small isolated particles and within troilite grains (fig. S19). Small native iron particles such as those that we have imaged within the silicate crystals [e.g., Fig. 3E and fig. S18D (2 and 4)] are predicted to be in the single domain (SD) or single vortex (SV) state and, hence, reliable Thellier paleointensity recorders (*31*) on billion-year time scales (*6*, *32*–*34*).

We note that because of the iron formation mechanism (*30*), replicating the oxygen fugacity of lunar basalts during paleointensity experiments is expected to promote the formation of new particles, inconsistent with reliable paleofield estimation (*6*). Instead, the principal requirement for paleointensity analysis using heating is choosing a method during which the magnetic grains can be considered stable. Accordingly, we focus on kinetics and select CO_2 laser heatings in air (see Materials and Methods). Specifically, this method has the dual advantages of best replicating the physical process of interest, that is, the acquisition of a TRM, whereas the brief CO_2 heating, 20 to 50 times shorter than conventional oven heatings, is least likely to induce chemical or structural change of the magnetic carriers. We again select 590°C, which is a temperature less than at which iron might sinter (*6*) but high enough that a range of unblocking temperatures are represented. We also note that 590°C is within the unblocking temperature range of the component identified as carrying the characteristic remanent magnetization (ChRM) in the few prior studies of Apollo samples using thermal methods.

All the crystals examined had very weak magnetizations (3.9×10^{-12} to 1.2×10^{-12} A m^2). However, we found that in each case, the magnetization after heating to 590°C did not yield consistent directions. This suggests that any remaining magnetization is (a) at a level below the magnetometer sensitivity or (b) that there was never a remanent magnetization imparted, and the NRM value reflects only a spurious viscous component. Magnetization measuring thresholds (Fig. 3, F and L, and figs. S17 to S20) support interpretation (b). Notwithstanding this early indicator of null ambient lunar fields, we proceed to further investigate the recording fidelity of the crystals by applying a TRM at 590°C in a 20-μT field. Twelve of the crystals acquired a consistent magnetization. We conclude that the one sample that did not acquire a remanence does not have recording properties able to report high fields, but the others do. For these, we can further estimate a maximum paleofield value that could be suggested by the data, assuming interpretation (a) (see Materials and Methods). These range from 0.6 to 2.8 μT (Fig. 3, F and L, and figs. S17 to S20), but as maxima and considering the caveat of assumption (a), these small values are indistinguishable from zero (see Materials and Methods).

As a further test, we reheat each sample to 590°C in zero field and then in the presence of a 40-μT field. The zero-field measurement, when referenced to the first zero-field measurement at 590°C (see Materials and Methods), show extraordinarily small differences (1.22 ± 0.97%), indicating a lack of alteration and a dominance of SD or SV grains, both consistent with our SEM results. The measurement after heating in a 40-μT field, when referenced to the intensity measured after the application of the field at 20 μT, provides a way to more directly evaluate the ability of each sample to record high, dynamo-like fields. Specifically, perfect recorders should yield a twofold increase in remanent intensity. We find that of the 12 crystals that recorded a laboratory field, the average efficiency (see Materials and Methods) of recording this Earth-like field intensity is 92 ± 11% (Fig. 3, F and L, and figs. S17 to S20). Thus, if a high dynamo-like field had been present on the Moon, then these samples should have recorded that field, but instead, they carry no appreciable magnetization.

DISCUSSION

Our five samples, indicative of negligible fields, span in age the prior suggested episodes of high lunar dynamo and late lunar dynamo and are supported by results from 11 other Apollo samples (Fig. 4 and table S5) within this age range, consistent with null lunar fields. Together, these data indicate that the Moon lacked any long-lived dynamo after ~4 Ga. We conclude that if other reported high nominal paleointensity values are not related to strong magnetic interactions, which can result in magnetizations that are not true paleofield signals (*35*), they were likely magnetized by a combination of shock (*36*) and impact fields. As noted earlier, the charge separation process depends on several factors, including impactor composition, velocity, angle, and dust generation. Therefore, not all shocked rocks are expected to have high imparted magnetizations. However, numerical simulations (*26*) indicate that impactors with radii ≤100 m are adequate to explain all the nominal "high-field epoch" values (Fig. 4). We note that these high values correspond in time to the later part of heavy bombardment (see Materials and Methods), the earlier period being in part or wholly obscured because the crust is near saturation levels of impacts (Fig. 4).

The lack of a long-lived lunar dynamo resolves the numerous and profound conflicts between the long-lived dynamo posit and lunar geology, crustal magnetizations, and dynamo driving mechanisms. A thermochemical driven dynamo in the first ~100 Ma of lunar history is feasible because of rapid cooling and has some support from crustal anomalies (*8*), which may reflect a vestige of this magnetization, complicated by the subsequent complex and intense impact history of the Moon. Such an early field could have contributed to the shielding of Earth from the solar wind (*3*). However, the Apollo samples examined here indicate that for most of its history, including times in the Paleoarchean when intense solar forcing could have led to terrestrial water loss (*4*, *37*), the Moon lacked a core dynamo and thus could not have provided additional magnetic shielding.

The lack of a lunar core dynamo also means that a magnetosphere would not have been present in the past to deflect ions (*4*) that could contribute to the volatile budget of the lunar surface. These charged particles would have two principal sources: the solar wind and Earth's atmosphere. The transfer from Earth's atmosphere would have occurred in the past as today (*38*) when the Moon passed through the magnetotail of Earth's ancient magnetosphere (*37*, *39*).

Saturation in solar wind volatiles by fine-grained regolith at the surface may occur more rapidly than the billion-year time scales considered here (*40*), and impact gardening can expose soils to the surface on time scales of hundreds of millions of years (*41*). However, some regions of the Moon have regolith >15 m deep (*41*), and these likely contain buried soils (*42*) that have not been recycled to the surface since ~1 Ga, the end of the erstwhile long-lived lunar dynamo, or much earlier times. We predict that these deep lunar soils represent a rich volatile reservoir, reflecting a ~4-Ga-old history of ion transport that can be explored by new missions such as Artemis. These volatiles include ^{3}He, water, and nitrogen, which could provide data on solar wind variability (*42*) and on the composition of Earth's early atmosphere. Overall, the absence of a long-lived dynamo

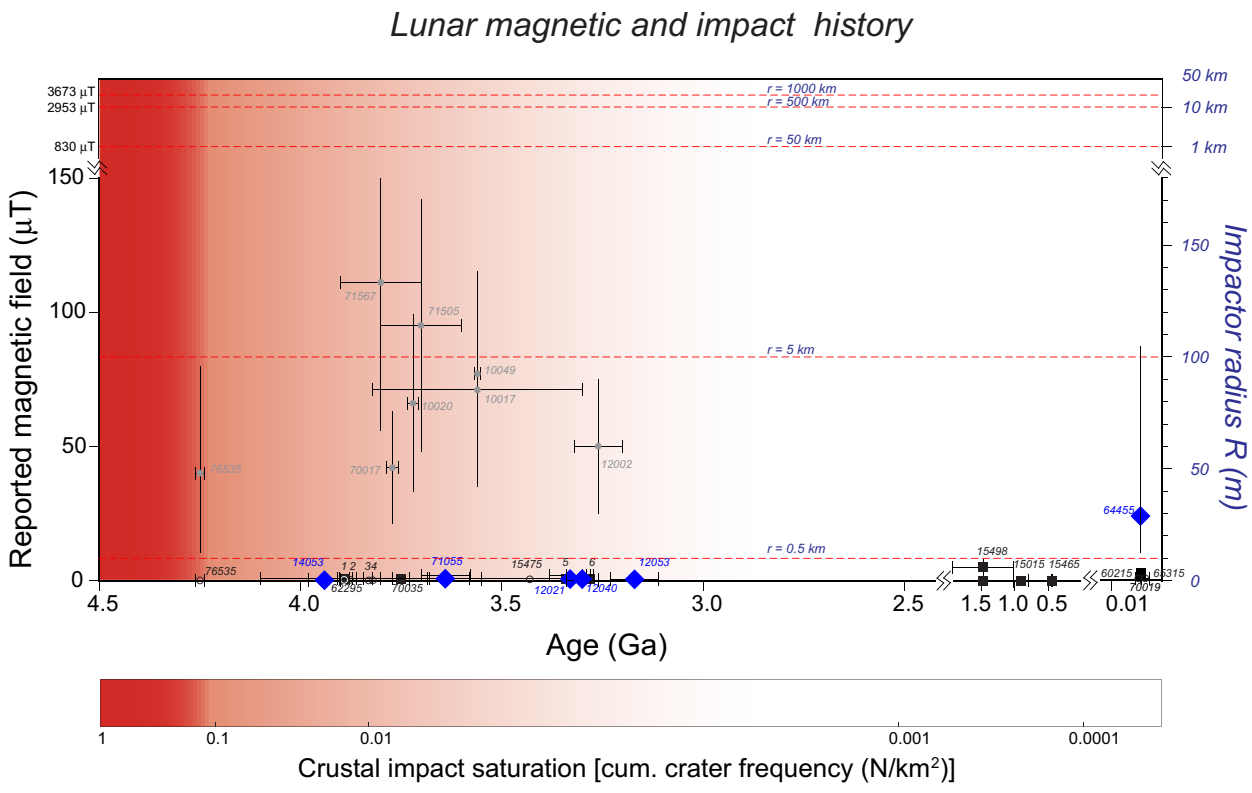

Fig. 4. Lunar magnetic and impact history. Reported field strength measurements from select Apollo samples (table S5) shown as follows: gray filled circles, nonthermal methods; open circles, no evidence for primary remanence, interpreted as magnetic contamination or results of magnetic interactions/phase changes during analysis; black squares, data based on thermal analyses. All sample numbers are listed except the following: 1, 68815 (open circle); 2, 62235; 3, 72215; 4, 75055; 5, 60015 (black square); and 6, 15016. Blue diamonds, thermal analysis values (this work). The right axis shows field impactor radius (*R*) capable of generating the field intensities by magnetizations induced by charge separation. Radius (*r*) values shown by dashed lines are field values at $r = 50R$. The shaded region reflects the degree of crustal impact saturation (see Materials and Methods).

indicates that the accumulation of volatiles was not limited by the shielding of a paleomagnetosphere, and this favors resource estimates suggesting that billions of kilograms of ^{3}He are preserved in the lunar regolith (*4*, *43*).

MATERIALS AND METHODS

The following sections describe methods and materials for Apollo samples measured; rock magnetic and light and electron microscope analyses; prior paleointensity analyses; and associated debate on methods, paleointensity measurements, and impact modeling and its interpretation with respect to imparted magnetizations.

Apollo samples analyzed

Crystals were selected such that they lacked large opaque mineral inclusions that could be multidomain iron. This application differs from other single-crystal studies (*44*) where crystals lacking any visible inclusions are selected. This revised selection criterion is necessary because of the common occurrence of the opaque mineral ilmenite in the lunar samples. Here, we seek to limit visible opaque inclusions, but in most cases, these cannot be eliminated entirely. Crystals from the following samples have been studied.

Apollo 16 sample 64455 is a basaltic impact melt (*17*) interpreted to have maintained its orientation since emplacement on the lunar surface. The ~5 cm–by–3 cm ovoid-shaped sample (fig. S2) consists of a relatively thick black glass rim with a delicate smooth exterior covering a basaltic melt interior. The glass is not an impact melt splash that might refer to melt coating a fixed rock but, instead, a coating acquired during ballistic transport of the rock and molten melt produced by the impact (*45*). The young exposure age is well constrained by several cosmogenic isotope systems. The ^{81}Kr exposure age is 2.01 Ma (*46*); the ^{21}Ne cosmic ray exposure age is 1.2 Ma, and the ^{36}Ar age is 1.8 Ma (*47*). The distribution of microcraters and ^{10}Be activity indicate an exposure age of 2 Ma (*19*, *48*), which is the generally accepted value for the sample. Apollo 64455 is from a suite of 22 rocks that are thought to have originated from South Ray crater that together yield tightly clustered exposure ages of 2.01 ± 0.1 Ma (*17*, *49*). Given the geology of the collection site, the physical nature of the sample, the consistency of the cosmogenic ages, the similarity with other Apollo 16 impact glasses linked to South Ray crater, and geochemical inferences for a local origin, we concur with prior authors (*45*, *50*) who concluded that it is most probable that an impact at 2 Ma formed the South Ray crater and the 64455 glass. It is possible that future ^{40}Ar-^{39}Ar dating of sample 64455 might help refine its age. However, in light of the rapid melting-and-quenching thermal loop experienced by lunar impact glasses, it has been suggested that insufficient Ar degassing will prevent age resetting (*45*, *51*) and, thus, that bulk-glass ^{40}Ar-^{39}Ar ages will reflect those of the target material. For instance, in the specific case of Apollo sample 64455, it has been shown experimentally that the outermost glass layer has a liquidus

of ca. 1400°C and that it must have cooled rapidly from this temperature, at approximately 140 K/min, to explain the general lack of devitrification and results from differential thermal analysis (*52*). Given these constraints and using the experimental parameters for Ar diffusion in basaltic melts (*53*), a characteristic temperature for Ar diffusion can be estimated at ca. 1180°C. For a 2-mm-thick melt layer, which is the minimum observed in sample 64455 (*54*), a total loss of Ar less than 3% is predicted, with substantial age resetting (>50%) restricted to only the outermost ca. <40 μm of the glass. Thus, only the outermost surface of the glass not substantially ablated by micrometeorites might preserve a glass formation age. In our paleointensity analyses, we focus on glass subsamples (Fig. 1A) from NASA Apollo sample "64455,24" (fig. S2) taken from the bottom of 64455, sheltered from micrometeorites (*17*).

Apollo 14 sample 14053,262 is a coarse-grained high-Al basalt, which is unusual relative to other lunar basalts because it is reduced during what has been interpreted to be a secondary event such as residence in an ejecta blanket (*55*). Specifically, our sample is from the outer, reduced portion of the 14053. It was proposed that 14053 represents an impact melt (*56*–*57*), but detailed trace element analyses indicate that it crystallized from a primary magma (*58*–*59*). An ^{39}Ar-^{40}Ar plateau age of 3.94 Ga (*60*) has been reported for 14053, as well as a Rb-Sr age of 3.96 Ga (*61*). On the basis of the similarity of these ages, we follow (*62*) in concluding that the inferred high-temperature reduction event occurred close to, or at, the time of the Ar-Ar plateau age (i.e., 3.94 Ga).

Several prior works discuss magnetizations from bulk samples of 14053 (*36*, *63*–*67*). The work in (*36*) focuses on a magnetization thought to be held at low unblocking temperatures (<300°C), and the authors conclude that the magnetization of their bulk samples was possibly carried by cohenite [$(Fe,Ni,Co)_3C$]. On the basis of a series of hydrostatic loading experiments to explore a piezoremanent magnetization that might mimic a shock remanent magnetization, these authors suggested that the NRM might be a shock remanent magnetization acquired in a field of 40 to 60 μT. In (*67*), a "partial TRM" recording of a somewhat lower strength field (20-μT field) was offered as an alternative interpretation of the data.

However, the suggestion of a cohenite carrier contrasts with early studies that highlight the relatively high iron content of 1.02 wt % and interpretations that multidomain native iron carriers were present (*62*–*63*). The presence of an iron carrier is strongly supported by the definition of maximum unblocking temperatures between 750° and 780°C (*63*). These contrasting interpretations may, at least in part, reflect the location of different subsamples analyzed from sample 14053; the main mass shows differences in the degree of reduction (*55*).

The differences between the analyses conducted here and those of previous studies of 14053 extend beyond the potential for specimen level differences in magnetic behavior. Our analyses are from small silicate crystals versus bulk samples and thus exclude large multidomain grains. This may explain the absence of any strong apparent magnetization seen in our specimens. Namely, the bulk samples may predominately record either spurious magnetizations or preferentially record shock remanent magnetization because their magnetic mineral assemblages are dominated by multidomain grains.

Apollo 12 sample 12021,30 is a coarse-grained porphyritic pigeonite basalt with large (up to 10 mm) pyroxene phenocrysts (*68*–*69*). It has a 3.3-Ga age based on Rb-Sr analyses (*70*–*71*).

Apollo 12 sample 12053,283 is a porphyritic pigeonite basalt (*72*–*73*). A whole rock Ar-Ar plateau yields an age of 3.17 Ga (*74*).

Apollo 12 sample 12040,209 is a coarse-grained olivine basalt (*69*, *75*); melt inclusions have been reported in silicate grains (*76*). It has a Rb-Sr age of 3.3 Ga (*71*, *77*).

Apollo 17 mare basalt 71055,2 is a "vesicular, fine- to medium-grained olivine-bearing ilmenite basalt" (*78*). It has a Rb-Sr age of 3.6 Ga (*79*).

Rock magnetic methods and analyses

Magnetic hysteresis data, including FORC data (*80*) were collected using a Princeton Measurement Corporation Model 2900 Alternating Gradient Force Magnetometer at the University of Rochester. FORC data were smoothed (*81*–*82*) using FORCinel version 3.01 and VARIFORC software.

Light and electron microscope methods and observations

Light stereomicroscopy was performed with a Nikon SMZ800 with a trinocular head, a maximum ×630 magnification, and a Spot Insight 4MP CCD color digital camera assembly. A Nikon Eclipse LV100POL was also used for both transmitted and reflected light microscopy. Glass subsamples and basalt single silicates were prepared in polished acrylic mounts, carbon-coated, and examined using a Zeiss Auriga SEM with an energy dispersive x-ray analysis (EDAX) energy dispersive spectrometer at the University of Rochester Integrated Nanosystems Center. Our Apollo 64455 glass sample is relatively uniform, and therefore, the subsamples that we selected for SEM analyses should be representative of those used for paleointensity analyses. Single silicate crystals from other Apollo samples are, in comparison, more variable in composition. Thus, we conducted an SEM examination of a specific crystal from each sample used in paleointensity analyses after the four brief (90 s) 590°C thermal treatments. We note that there is no textural evidence in our light microscope or SEM observations to indicate that the Apollo 64455 Fe-Ni-S spheres were incorporated into the glass after its formation. Hence, these spheres are primary magnetic inclusions. Our SEM observations on the lunar single silicate grains show an occurrence of magnetic inclusions that are similar to magnetic grains seen in bulk lunar basalt samples (*30*) but with sizes that are orders of magnitude smaller. Hence, the single silicates are more suitable than bulk samples for recording paleointensities (*29*, *31*).

Prior paleointensity analyses: Debates over methods and interpretations

It is commonly accepted that to obtain accurate past field records, lunar samples carrying TRMs should be sought (*83*). However, what may be underappreciated is that most available sample data used to estimate lunar paleointensity rely on nonthermal methods that do not directly test Thellier's laws and, hence, the presence of a TRM (*6*). Accordingly, there has been considerable concern over the use of nonthermal methods to estimate paleointensity (*9*), to the point that they have been called "the methods of last resort" (*6*). The concern is punctuated by the multiple assumptions that must be made estimating a TRM quantity (i.e., paleointensity) using a process different from that which imparted any original magnetization. Nonthermal methods ultimately rely on an assumption that magnetic coercivities explored by the application of laboratory AFs equate with magnetic blocking temperatures. Ideally, this need not be an assumption if quantitative information on magnetic domain

state distributions is available and linked uniquely to magnetic coercivities and blocking temperatures, but this quantitative information and attendant linkages are unavailable.

In the absence of a core dynamo, lunar samples might still hold a viscous magnetization and an NRM; that is, the sample might record a measurable magnetic moment before demagnetization. However, a key discriminating property is that in the absence of a core dynamo, samples should not yield a ChRM, which is a component obtained after demagnetization of any viscous contamination. Thus, a signature of the lack of a core dynamo is the observation of directional instability after viscous components have been reported after relatively low AF or thermal demagnetization treatments. Several prior studies have reported unstable AF and/or thermal demagnetization behavior of lunar samples, consistent with the lack of a field.

However, bulk lunar magnetic samples typically contain large multidomain magnetic (MD) grains, and these are thought to be unstable during the application of AFs, demagnetization, or the application of anhysteretic fields [anhysteretic remanent magnetizations (ARMs)]. Hence, separating the influence of laboratory-induced noise from evidence for a null remanence is often not straightforward when nonthermal methods (i.e., AFs) are used.

ARM data have been used to assess the recording reliability of lunar samples (*84*). In this method, an ARM is applied at different bias fields and then used to compute paleointensities, assuming a calibration (*85*). For some samples, the quality of the paleointensity determination and its agreement with the known applied field decreased as the magnitude of the applied field was decreased. The applied field value when differences between the expected and obtained paleointensities are greater than 100% and/or the errors in the paleointensity exceed 100% is called a minimum paleointensity that can be recorded by the sample using this ARM method (*84*). The study outlining this approach includes a discussion of the limitations of the equipment used for AF demagnetization and ARM acquisition and the problems with harmonics in the signals (*84*). However, while the noise introduced into measurements is well documented, the extension of the ARM measurements to the general conclusion that a given sample cannot record a field below the ARM method minimum (*86*), or, furthermore, that such samples provide no evidence for the absence of a core dynamo (*87*), is not justified as we explain below.

Within the context of a planetary body where the primary question is the absence or presence of an internally generated magnetic field, the lack of a characteristic magnetization is, to first order, the evidence for the lack of a field, provided that the sample contains magnetic grains capable of recording fields on the requisite time scales (i.e., equal to or older than the age of the sample in question). To demonstrate that the lack of a stable magnetization is not evidence for the lack of a magnetic field, one would need to prove that there are no grain sizes/domain states present that could record and retain that field. Although multidomain grains are reported (but not illustrated) in microprobe analyses reported in (*84*), FORC diagrams from the same samples clearly indicate another pseudosingle domain or single vortex component [figure S5 of (*84*)]. These are grains that could retain fields on the billion year time scales relevant to the Moon.

If MD grains are present, the application of AF tends to exacerbate experimental noise. The ARM work of (*84*), in which experimental noise is present and acknowledged, has been further extended to claim that some lunar samples can only record a field as low as that defined by their ARM error analysis [in the case of Apollo 15016, the claimed minimum is 37 μT; (*86*)]. Instead, these experiments show only that ARM methods are poorly suited for robust paleointensity estimates in the samples. The rock magnetic demonstration that magnetic grains capable of recording a TRM are present and the lack of a ChRM together suggest that these samples passed through their blocking temperatures or were shocked in the absence of an ambient field. Therefore, in our summary of magnetic directions, we include a select set of samples analyzed by prior authors (cf., table S5) where no ChRM was present.

Two prior debatable interpretations figure largely in the posit of a long-lived dynamo. These are the oldest and youngest samples proposed to record the field. For the youngest sample, specimens record both a measurable paleofield and no field (*14*). The sample investigated (Apollo 15498) is a complex impact breccia with basaltic clasts, a glass matrix, fissures filled with vesicular glass, and a coating of "splash" glass a few to 6 mm thick (*88*). There are different interpretations of the origin of the matrix glass. In one, this results from in situ high-pressure shock that is evident by a wide variety of shock features (e.g., shock lamellar structures), with the lack of unshocked clasts providing evidence for an in situ origin (*89*). In another interpretation, the glass matrix is thought to have originated as an impact melt that underwent high-temperature rapid cooling followed by a slower cooling (*90*), with evidence for this process rather than shock provided in the form of experimental analyses of annealing characteristics (although no counter argument against the absence of unshocked clasts is provided).

A paleointensity of a few microteslas using a modified Thellier technique was originally reported on this sample (*91*) and confirmed in the restudy (*14*), which focused on glassy matrix samples, but in the restudy, specimens within 2 cm of the contact with the splash glass lacked a ChRM. These specimens were interpreted to have been demagnetized in a later null field (*14*) and that only interior samples recorded a core dynamo. It was argued that the remanence of these interior specimens was acquired slowly, on hour time scales, i.e., longer than the time scales of magnetization by impacts that were claimed to be <~1 s (specifically for impacts after 3.3 Ga; Supplementary Materials) (*14*). However, the remanence acquisition and impact field time scales are incorrect, as described below.

Irrespective of uncertainty over its mode of formation described earlier, there is an agreement that the glass matrix cooled very rapidly to temperatures as low at ~620°C. In (*14*), a conductive cooling model is used to conclude an hour time scale to reach ambient lunar conditions, but this end point is not relevant to the magnetization of 15498. Instead, the relevant time is only that to span the blocking temperature range represented by the ChRM. In reference to the data highlighted [figure 7 of (*14*)], a "high temperature" component is defined that appears to span temperatures from high to low temperatures, but this component does not correspond to the temperatures used in the paleointensity estimates. Specifically, the component yielding a nonzero field is isolated only after heating above 560°C. The lowest unblocking temperature where a field is recorded is within ~60°C of the nominal temperature change from extremely rapid to slow cooling. Given the uncertainties in these analyses related to the unquantified complexities of the cooling (*90*) and the uncertainties in uniquely relating magnetic unblocking to ambient temperatures in the breccia, we consider this difference to be within error, and we thus conclude that the glass matrix from sample 15498 could have acquired its magnetization on minute time scales. Moreover, we note that the paleointensity isolated at lower temperatures (250° to

540°C) is essentially null (0.2 ± 0.1 μT). This is interpreted as a partial shock demagnetization, at a shock level that left no evidence of the event (*14*). Instead, this change from a magnetized to unmagnetized sample could represent either the rapid decay of a transient field produced by an impact by charge separation and/or the physical transport of the sample out of the range of a strong magnetizing field.

The dismissal of impact magnetizations based on a lower frequency of large impacts after 3.3 Ga in (*14*) is inconsistent with the potential crater sources. Specifically, both Aristillus (diameter, 55 km) and Autolycus crater (diameter, 39 km) have been discussed as sources of ejecta and secondary craters near the Apollo 15 site, where sample 15498 was collected (*92*). These craters are very far from the collection site (>180 to 130 km), so quenching of the glass during transport and magnetization is likely; impactors responsible for these craters could have generated fields many hundreds of microteslas in strength through charge separation (*26*–*27*), which can explain the observed nonzero paleointensity values. We again note that the outermost glass of 15498 is unmagnetized and is interpreted in (*14*) to record a separate, later event in a null field. Alternatively, the glass emplacement may be related to the final emplacement of the sample in a secondary impact insufficient to drive substantial charge separation. Thus, we conclude that the magnetization characteristics of 15498 provide no conclusive evidence for a dynamo at 1.5 Ga but instead are better explained by impact processes.

The oldest sample purported to record a lunar dynamo, the 4.2-Ga-old coarse-grained troctolite 76535 (*93*), has a history inherently related to one or more impacts because these are needed to bring the sample to the surface from a great depth (*94*). The magnetism of this sample was first studied in (*9*), and it was noted that the removal of almost 80% of the signal occurred by 540°C, with a unidirectional signal. However, pTRM checks failed at high and low temperatures, and at high temperatures (the experiment was ceased at 770°C), the sample was not losing NRM/gaining pTRM in a pattern consistent with a TRM. Similarities in the magnetic behavior were noted relative to other lunar samples, specifically where NRM/TRM characteristics at low temperature were linked to magnetic interactions and where those at higher temperatures were due to the formation of new iron phases. This behavior suggests that the signal might not be an accurate recorder of any ambient lunar field.

Subsequently, paleointensities were reported for 76535 using nonthermal techniques, where it was argued that the slow cooling and magnetization required a core dynamo (*10*). Ambiguity in the internal consistency of specimens studied motivated a second study using similar nonthermal techniques (*95*). The identified high-coercivity component is very noisy; the directions define a cloud of points with numerous instances where magnetization increases rather than decreases with demagnetization, only to decrease at the next demagnetization step. This appears to reflect the acquisition and subsequent removal of AF artifacts, but after so many of these spurious signals are imparted to each specimen [>30, figure 5 of (*95*)], there are concerns over the meaning of any derived direction. Concomitant with this noise, we see that the method of constraining a fit to the data such that it must pass through the origin of an orthogonal vector plot has a very large influence on the assigned uncertainty. Without this constraint, the nominal high coercivity components assigned to two of the three specimens studied have median angular dispersions so high (41° and 32°) that they would not be acceptable in studies of terrestrial materials. The third specimen yields a high, marginal value (29°). The high uncertainties of the fits prevent any conclusive determination that the specimens record a common direction indicative of a TRM.

Beyond the low quality of the AF directional data, major unresolved issues revolve around equating the coercivity spectra of the specimens with the apparent thermal unblocking defined in (*9*) and whether any signal could record an impact field. Specifically, in (*10*) and (*95*), the nominal high coercivity component is related to very high blocking temperatures typical of kamacite and the unblocking temperatures reported in (*9*). However, in (*9*), it was cautioned that the characteristics might relate to iron formation by ilmenite reduction in the laboratory. Moreover, the textural evidence for slow cooling in 76535 does not require any magnetization that it holds to be acquired over long durations, contrary to claims in (*10*) and (*95*). A large impact is needed to bring 76535 to the surface. If this impact occurred at ~4.2 Ga, then the sample could have been exposed to a large field produced by charge separation, with its magnetic minerals rapidly passing through their Curie temperatures and acquiring a magnetization in the absence of a core dynamo.

Paleointensity methods and analyses

Glass samples and single silicate crystals were mounted in 2 mm–by–2 mm–by–2 mm fused quartz boxes and set with a minimum of sodium silicate solution for all remanence measurement. The purity of these materials has been documented by use of a scanning superconducting quantum interference device (SQUID) microscope (*96*–*97*). Paleomagnetic measurements were made using an ultrahigh-resolution 6.3-mm-bore William S. Goree. Inc. (WSGI) three-component DC SQUID magnetometer in the magnetically shielded room at the University of Rochester (ambient field, <200 nT). This magnetometer affords an order of magnitude greater sensitivity than other 2G SQUID magnetometers.

Thermal analyses

For TTRM (*98*) and Thellier-Coe experiments of 64455 glass, specimens were heated in air using a Firestar V20 CO_2 laser (also in the University of Rochester's magnetically shielded room). Thermal paleointensity techniques follow those developed for single-crystal paleointensity analysis (*29*, *39*, *44*, *97*, *99*). The heating time used to evaluate alteration using magnetic hysteresis was 3 min. Heating times for each paleointensity step were either 90 s (subsamples <1 mm in size) or 120 s (subsamples 1 to 2 mm in size). For one TTRM experiment (subsample ss40), we used a three-point sliding window for the orthogonal vector plots to reduce noise and identify the temperature range of the ChRM. For Thellier data, we use the following reliability criteria (*99*). A sample is deemed successful if there is a linear relationship between the loss of NRM and the acquisition of a laboratory-induced magnetization (R^2 value generally greater or equal to 0.9). Four or more points should define the best-fit line. NRM-TRM points should be evenly distributed along the best-fit line, and pTRM checks should fall within 15% of the original value. The maximum angular deviation should be less than 15 degrees, and the field-off steps should not trend in the direction of the applied field. We have relaxed these criteria somewhat for our lunar results relative to terrestrial samples (allowed for greater maximum angular deviation (MAD) angles and deviation of the pTRM checks), and for two subsamples (ss31 and ss42), we used a three-point sliding window for the orthogonal vector plots to reduce noise and identify the ChRM temperature range.

For TRM analyses of Apollo basalt silicates at 590°C, we use the specimen preparation, CO_2 laser, and magnetometer as described

above, with all heating times at 90 s. These measurements are similar to those conducted at 565°C on terrestrial zircons (*39*, *97*) but differ in one key way. At 565°C, terrestrial zircons have a stable magnetization with a paleointensity that is within a factor of two of Thellier data that uses the full unblocking spectra of the ChRM. In contrast, the lunar silicate crystals examined here lack a ChRM that should otherwise be represented by stable magnetic direction after heating at 590°C (in zero field). After heating to 590°C in 20 μT, we reheat the lunar silicates in zero field to conduct an MD-tail test [see Methods in (*39*)]. After heating lunar silicates in 40 μT, we define the TRM efficiency as

$$\frac{M_{590,40\mu T}}{M_{590,20\mu T} \times 2} \times 100$$

where $M_{590,40\mu T}$ and $M_{590,20\mu T}$ are the magnetizations imparted in applied fields of 40 and 20 μT, respectively.

Nonthermal analyses

Nonthermal paleointensity use the REM' method, which is thought to be best suited for samples that might show multicomponent magnetizations (*100*). The slope of NRM data demagnetized by AF was normalized by the slope of demagnetization data of the SIRM data. The demagnetization segment chosen for paleointensity determination is that which defines the component deemed to be primary. After measurement of the NRM, samples were AF-demagnetized up to 300 mT. The order of AF demagnetization axes with progressively higher peak fields was permutated (*101*) to counter any acquisition of a gyroscopic remanent magnetization. Following demagnetization of the NRM, the sample was given an SIRM in a 3-T field using an ASC Scientific Impulse Magnetizer. The initial SIRM was measured, followed by AF demagnetization using the same step procedure used and axis permutations for the AF demagnetization of the NRM. A smoothing-interpolation method (*101*) was applied to the NRM and IRM demagnetization data, again to mitigate any effects of GRM. A comparison of the loss of NRM to the loss of IRM [ratio of equivalent magnetizations (REM)] can be used to estimate for paleointensity of the sample. Orthogonal vector plots of NRM and IRM demagnetization were used to determine the AF demagnetization range of the component of magnetization most likely to be of primary origin. Calibration compilations (*100*, *102*–*103*) suggest that the paleofield (B_o, in tesla) is equal to the $\sim 3.01 \times 10^{-3}$ REM for single to multidomain magnetite and titanomagnetite. FeNi alloys and lunar samples have been interpreted to be compatible with this trend (*100*).

In considering uncertainties for our nonthermal analyses, we follow the usage in prior works that assign a factor of two uncertainties to calibrations. We view this as a minimum uncertainty. For the 64455 glass, there are other calibration data that might be applied on the basis of experiments producing small iron spheres (see table S4). These calibrations yield a different range (low field bound of 4 versus 10 μT; high field bound of 82 versus 89 μT) that does not affect the conclusions here.

Impact modeling, interpretations, and history

Modeling of South Ray crater was done using the code iSALE2D (*104*–*105*). Our input files are included as data files S1 and S2. We use a dunite impactor, which is also assumed in the Crawford model (*26*). We choose granite as a target material because it has properties more similar to lunar anorthosite and better approximates the target considered in Crawford (*26*). The impact velocity (14 km/s) is chosen as the vertical component of an impact velocity of 20 km/s with an impact angle of 45°. Impacts can create charge separation (*26*, *106*–*107*) because they generate a combination of debris and ionized gas (plasma). The probability of electron interaction with impact debris is higher than that for ions, and, in turn, more electrons bind to the debris, making it negatively charged. As the debris leaves the impact site, it carries away this negative charge, leaving a slightly positively charged plasma. The net charge increases with the impactor mass and velocity. This charge then produces an electric field, which, in turn, drives a current that induces a magnetic field; experiments corroborate this effect (*107*). Detailed simulations confirm (*26*) the mechanism outlined above and provide the scaling for the amplified surface field.

A recent modeling study (*25*) of the hypothesis whereby impacts generate antipodal magnetic anomalies by compression of the solar wind magnetic field (*24*) also comments on the charge separation process. Specifically, the work in (*25*) cites four papers (*108*–*111*) and states "numerous paleomagnetic investigations of impact craters on the Earth have found that impact-heated rocks record the background field and found no evidence of an amplified or locally generated transient field." This statement does not properly represent the cited literature. First, in the study of the Vredefort impact structure cited (*108*), the authors argue that lightning remagnetizations prevent recognition of impact magnetizations. Second, in a review of crustal anomalies from several terrestrial impact craters, the authors of (*109*) note that there are anomalous high signals but that these might be explained by high ferromagnetic mineral contents. Otherwise, the work focuses on melt rocks, specifically with the goal of determining whether impacts could affect the geodynamo rather than testing with paleointensity analyses whether impact fields are recorded. However, in a discussion of the small ~1.8-km-diameter Lonar crater of India, the authors of (*109*) note that evidence of shock remanent magnetization is "hotly debated." They further note that in a magnetic study of the Lonar crater (*110*), the third study cited by (*25*), the subsequent acquisition of viscous and/or chemical magnetization in Earth's field prevented recognition of a shock component. Therefore, rather than commenting on the charge separation magnetization process, these three papers instead explain why it is so difficult to recognize impact magnetization on Earth. One recorder that might be able to record such fields is impact glasses, magnetized on short times similar to those of Apollo 64455. The fourth cited work (*111*) studied tektites from the Lonar crater, which might record such fields. There are sampling shortcomings in the work in that some samples appear to be weathered and/or are not pure glass. In addition, the method chosen, NRM/SIRM (versus REM'), is thought to provide only order-of-magnitude estimates of paleointensity (*6*). Nevertheless, the authors concluded that no fields >~100 μT were observed, that these were orders of magnitude less than those predicted by (*107*), and that, therefore, the Lonar tektites provided a counter example to locally strong impact-induced fields resulting from the charge separation process. However, in a more recent study (*26*), the electrostatic charge model was revised with Mg^+ rather than Ca^+ being the dominant ion source; the higher ionization energy ultimately results in lower field values. A 35-m-radius impactor is called upon to form the Lonar crater (*111*). Charge separation (Eq. 1) predicts fields of 29 μT at 50*R*. The recent field intensity at the site is ~44 μT, which was probably similar during the time of the impact, dated at ~0.57 Ma (*112*) during the Brunhes

chron. Thus, while some of the values reported in (*111*) from their "large" samples nominally agree with the charge separation predictions of (*26*), the similarity of the predicted and geodynamo fields and the inaccuracy of the paleointensity method applied prevent any meaningful test. Overall, while the terrestrial environment is challenging for examining charge separation given the background field and other crustal process that can enhance bulk magnetic mineral content at impact sites (e.g., hydrothermal circulation), we hope that our results from Apollo 64455 will motivate new and more detailed magnetic examinations of impact craters and ejecta on Earth.

The abundance of small and large lunar craters that we refer to is derived from (*113*) and (*114*). We rely on (*115*) and (*116*) to derive the impact frequency shown in Fig. 4.

SUPPLEMENTARY MATERIALS

Supplementary material for this article is available at http://advances.sciencemag.org/cgi/content/full/7/32/eabi7647/DC1

REFERENCES AND NOTES

1. S. M. Cisowski, D. W. Collinson, S. K. Runcorn, A. Stephenson, M. Fuller, A review of lunar paleointensity data and implications for the origin of lunar magnetism. *J. Geophys. Res.* **88**, A691–A704 (1983).
2. A. J. Evans, S. M. Tikoo, J. C. Andrews-Hanna, The case against an early lunar dynamo powered by core convection. *Geophys. Res. Lett.* **45**, 98–107 (2018).
3. J. Green, D. Draper, S. Boardsen, C. Dong, When the Moon had a magnetosphere. *Sci. Adv.* **6**, eabc0865 (2020).
4. J. A. Tarduno, E. G. Blackman, E. E. Mamajek, Detecting the oldest geodynamo and attendant shielding from the solar wind: Implications for habitability. *Phys. Earth Planet. Inter.* **233**, 68–87 (2014).
5. B. Fegley Jr., T. D. Swindle, Lunar volatiles: Implications for lunar resource utilization, in *Resources of Near Earth Space*, J. Lewis, M. S. Matthews, M. L. Guerrieri, Eds. (University of Arizona Press, 1993), pp. 367–426.
6. D. J. Dunlop, Ö. Özdemir, *Rock Magnetism: Fundamentals and Frontiers* (Cambridge Univ. Press, 2001).
7. S. M. Cisowski, C. Hale, M. Fuller, On the intensity of ancient lunar fields. *Proc. Lunar Sci. Conf.* **8**, 725–750 (1977).
8. M. A. Wieczorek, Strength, depth, and geometry of magnetic sources in the crust on the Moon from localized power spectrum analysis. *J. Geophys. Res.* **123**, 291–316 (2018).
9. K. Lawrence, C. Johnson, L. Tauxe, J. Gee, Lunar paleointensity measurements: Implications for lunar magnetic evolution. *Phys. Earth Planet. Inter.* **168**, 71–87 (2008).
10. I. Garrick-Bethell, B. P. Weiss, D. L. Shuster, J. Buz, Early lunar magnetism. *Science* **323**, 356–359 (2009).
11. E. K. Shea, B. P. Weiss, W. S. Cassata, D. L. Shuster, S. M. Tikoo, J. Gattacceca, T. L. Grove, M. D. Fuller, A long-lived lunar core dynamo. *Science* **335**, 453–456 (2012).
12. M. Le Bars, M. A. Wieczorek, O. Karatekin, D. Cébron, M. Laneuville, An impact-driven dynamo for the early Moon. *Nature* **479**, 215–218 (2011).
13. C. A. Dwyer, D. J. Stevenson, F. Nimmo, A long-lived lunar dynamo driven by continuous mechanical stirring. *Nature* **479**, 212–214 (2011).
14. S. M. Tikoo, B. P. Weiss, D. L. Shuster, C. Suavet, H. Wang, T. L. Grove, A two-billion-year history for the lunar dynamo. *Sci. Adv.* **3**, e1700207 (2017).
15. M. Laneuville, M. A. Wieczorek, D. Breuer, J. Aubert, G. Morard, T. Rückriemen, A long-lived lunar dynamo powered by core crystallization. *Earth Planet. Sci. Lett.* **401**, 251–260 (2014).
16. S. Mighani, H. Wang, D. L. Shuster, C. S. Borlina, C. I. O. Nicols, B. P. Weiss, The end of the lunar dynamo. *Sci. Adv.* **6**, eaaz0883 (2020).
17. G. Ryder, M. D. Norman, *Catalog of Apollo 16 rocks: Part 2 63335-66095* (Curatorial Branch Publication 52, NASA JSC 16904, 1980).
18. A. G. Sanchez, D4. Geology of Stone Mountain, in Geology of the Apollo 16 Area, Central Lunar Highlands, in *Geological Survey Professional Paper 1048*, G. E. Ulrich, C. A. Hodges, W. R. Muehlbergerm, Eds. (U.S. Gov. Print. Office, 1981), pp. 106–126.
19. K. Nishiizumi, C. P. Kohl, J. R. Arnold, R. C. Finkel, M. W. Chaffee, J. Masarik, R. C. Reedy, Final results of comogenic nuclides in lunar rock 64455. *Lunar Planet. Sci. Conf.* **26**, 1055–1056 (1995).
20. L. Tauxe, T. A. T. Mullender, T. Pick, Potbellies, wasp-waists, and superparamagnetism in magnetic hysteresis. *J. Geophys. Res.* **101**, 571–583 (1996).
21. M. Fuller, Lunar magnetism. *Rev. Geophys. Space Phys.* **12**, 23–70 (1974).
22. P. Dyal, C. W. Parkin, W. D. Dailey, Magnetism and the interior of the Moon. *Rev. Geophys. Space Phys.* **12**, 568–591 (1974).
23. H. Tsunakawa, F. Takahashi, H. Shimizu, H. Shibuya, M. Matsushima, Surface vector mapping of magnetic anomalies over the Moon using Kaguya and Lunar Prospector observations. *J. Geophys. Res.* **120**, 1160–1185 (2015).
24. L. L. Hood, N. C. Richmond, P. D. Spudis, Origin of strong lunar magnetic anomalies: Further mapping and examinations of LROC imagery in regions antipodal to young large impact basins. *J. Geophys. Res.* **118**, 1265–1284 (2013).
25. R. Oran, B. P. Weiss, Y. Shprits, K. Miljković, G. Tóth, Was the moon magnetized by impact plasmas? *Sci. Adv.* **6**, eabb1475 (2020).
26. D. A. Crawford, Simulations of magnetic fields produced by asteroid impact: Possible implications for planetary paleomagnetism. *Int. J. Impact Eng.* **137**, 103464 (2020).
27. M. Bruck Syal, P. H. Schultz, Cometary impact effects at the Moon: Implications for lunar swirl formation. *Icarus* **257**, 194–206 (2015).
28. N. Sugiura, Y. M. Wu, D. W. Strangway, G. W. Pearce, L. A. Taylor, A new magnetic paleointensity value for a 'young lunar glass'. *Proc. Lunar Planet. Sci. Conf.* **10**, 2189–2197 (1979).
29. J. A. Tarduno, R. D. Cottrell, A. V. Smirnov, The paleomagnetism of single silicate crystals: Recording the geomagnetic field during mixed polarity intervals, superchrons and inner core growth. *Rev. Geophys.* **44**, RG1002 (2006).
30. J. Papike, L. Taylor, S. Simon, Lunar minerals, *in Lunar Source Book*, G. H. Heiken, D. T. Vaniman, B. M. French, Eds. (Cambrige Univ. Press, 1991), chap. 5, pp. 137–153.
31. A. V. Smirnov, E. V. Kulakov, M. S. Foucher, K. E. Bristol, Intrinsic paleointensity bias and the long-term history of the geodynamo. *Sci. Adv.* **3**, e1602306 (2017).
32. A. R. Muxworthy, W. Williams, Critical single-domain grain sizes in elongated iron particles: Implications for meteoritic and lunar magnetism. *Geophys. J. Int.* **202**, 578–583 (2015).
33. T. P. Almeida, A. R. Muxworthy, A. Kovács, W. Williams, P. D. Brown, R. E. Dunin-Borkowski, Direct visualization of the thermomagnetic behavior of pseudo–single-domain magnetite particles. *Sci. Adv.* **2**, e1501801 (2016).
34. L. Nagy, W. Williams, L. Tauxe, A. R. Muxworthy, I. Ferreira, Thermomagnetic recording fidelity of nanometer-sized iron and implications for planetary magnetism. *Proc. Natl. Acad. Sci. U.S.A.* **116**, 1984–1991 (2019).
35. T. O'Brien, J. A. Tarduno, A. Anand, A. V. Smirnov, E. G. Blackman, J. Carroll-Nellenback, A. N. Krot, Arrival and magnetization of carbonaceous chondrites in the asteroid belt before 4562 million years ago. *Commun. Earth Environ.* **1**, 54 (2020).
36. J. Gattacceca, M. Boustie, L. Hood, J. P. Cuq-Lelandais, M. Fuller, N. S. Bezaeva, T. De Resseguier, L. Berthe, Can the lunar crust be magnetized by shock: Experimental groundtruth. *Earth Planet. Sci. Lett.* **299**, 42–53 (2010).
37. J. A. Tarduno, R. D. Cottrell, M. K. Watkeys, A. Hofmann, P. V. Doubrovine, E. E. Mamajek, D. Liu, D. G. Sibeck, L. P. Neukirch, Y. Usui, Geodynamo, solar wind, and magnetopause 3.4 to 3.45 billion years ago. *Science* **327**, 1238–1240 (2010).
38. K. Terada, S. Yokota, Y. Saito, N. Kitamura, K. Asamura, M. N. Nishino, Biogenic oxygen from Earth transported to the Moon by a wind of magnetospheric ions. *Nat. Astron.* **1**, 0026 (2017).
39. J. A. Tarduno, R. D. Cottrell, W. J. Davis, F. Nimmo, R. K. Bono, A Hadean to Paleoarchean geodynamo recorded by single zircon crystals. *Science* **349**, 521–524 (2015).
40. F. Hörz, R. Grieve, G. Heiken, P. Spudis, A. Binder, Lunar surface processes, *in Lunar Source Book*, G. H. Heiken, D. T. Vaniman, B. M. French, Eds. (Cambrige Univ. Press, 1991), chap 4, pp. 61–120.
41. H. J. Melosh, *Planetary Surface Processes* (Cambridge Univ. Press, 2011).
42. S. A. Fagents, M. E. Rumpf, I. A. Crawford, K. H. Joy, Preservation potential of implanted solar wind volatiles in lunar paleoregolith deposits buried by lava flows. *Icarus* **207**, 595–604 (2010).
43. W. Fa, Y.-Q. Jin, Quantitative estimation of helium-3 spatial distribution in the lunar regolith layer. *Icarus* **190**, 15–23 (2007).
44. J. A. Tarduno, R. D. Cottrell, M. K. Watkeys, D. Bauch, Geomagnetic field strength 3.2 billion years ago recorded by single silicate crystals. *Nature* **446**, 657–660 (2007).
45. R. V. Morris, T. H. See, F. Hörz, Composition of the Cayley formation at Apollo 16 as inferred from impact melt splashes. *J. Geophys. Res.* **17**, E21–E42 (1986).
46. J. R. Arnold, C. P. Kohl, K. Nishiizumi, M. W. Caffee, R. C. Finkel, J. R. Southon, Measurements of cosmogenic nuclides in lunar rock 64455, in *24th Lunar and Planetary Science Conference* (SAO/NASA Astrophysics Data System, 1993), 39 pp.
47. D. D. Bogard, E. K. Gibson Jr., Volatile gases in breccia 68115. *Lunar Planet. Sci. Conf.* **6**, 63–65 (1975).
48. K. Nishiizumi, J. R. Arnold, C. P. Kohl, M. W. Chaffee, J. Masarik, R. C. Reedy, Solar cosmic ray records in lunar rock 64455. *Geochim. Cosmochim. Acta* **73**, 2163–2176 (2009).
49. O. Eugster, Chronology of dimict breccias and the age of South Ray crater at the Apollo 16 site. *Meteorit. Planet. Sci.* **34**, 385–391 (1999).
50. T. H. See, F. Hörz, R. V. Morris, Apollo 16 impact-melt splashes; petrography and major-element composition. *Proc. Lunar Planet. Sci. Conf.* **91**, E3–E20 (1986).

51. B. A. Cohen, T. D. Swindle, D. A. Kring, Geochemistry and ^{40}Ar-^{39}Ar geochronology of impact-melt clasts in feldspathic lunar meteorites: Implications for lunar bombardment history. *Meteorit. Planet. Sci.* **40**, 755–777 (2005).
52. D. R. Ulrich, J. Weber, Correlation of the thermal history of lunar and synthetic glass by DTA and X-ray techniques. *Lunar Planet. Sci. Conf.* **4**, 743 (1973).
53. M. Nowak, D. Schreen, K. Spickenbom, Argon and CO_2 on the race track in silicate melts: A tool for the development of a CO_2 speciation and diffusion model. *Geochim. Cosmochim. Acta* **68**, 5127–5138 (2004).
54. R. A. F. Grieve, A. G. Plant, Partial melting on the lunar surface, as observed in glass coated Apollo 16 samples. *Lunar Planet. Sci.* **4**, 667–679 (1973).
55. L. A. Taylor, A. Patchen, R. G. Mayne, D. H. Taylor, The most reduced rock from the moon, Apollo 14 basalt 14053: Its unique features and their origin. *Am. Mineral.* **89**, 1617–1624 (2004).
56. G. A. Synder, L. A. Taylor, Oldest mare basalts or impact melts? The role of differential melting of plagioclase in Apollo 14 high-Al basalts. *Meteorit. Planet. Sci.* **36**, A194 (2001).
57. F. M. McCubbin, A. Steele, E. H. Hauri, H. Nekvasil, S. Yamashita, R. J. Hemley, Nominally hydrous magmatism on the Moon. *Proc. Natl. Acad. Sci. U.S.A.* **107**, 11223–11228 (2010).
58. C. R. Neal, L. A. Taylor, Petrogenesis of mare basalts: A record of lunar volcanism. *Geochim. Cosmochim. Acta* **56**, 2177–2211 (1992).
59. C. R. Neal, G. Y. Kramer, The petrogenesis of the Apollo 14 high-Al mare basalts. *Am. Mineral.* **91**, 1521–1535 (2006).
60. A. Stettler, P. Eberhardt, J. Geiss, N. Grögler, P. Maurer, Ar^{39}-Ar^{40} ages and Ar^{37}-Ar^{38} exposure ages of lunar rocks. *Proc. Lunar Planet. Sci. Conf.* **4**, 1865–1888 (1973).
61. D. A. Papanastassiou, G. J. Wasserburg, Rb-Sr ages of igneous rocks from the Apollo 14 mission and the age of the Fra Mauro formation. *Earth Planet. Sci. Lett.* **12**, 36–48 (1971).
62. J. R. Dunn, M. Fuller, On the remanent magnetism of lunar samples with special reference to 10048,55 and 14053,48. *Proc. Lunar Planet. Sci. Conf.* **3**, 2363–2386 (1972).
63. T. Nagata, R. M. Fisher, F. C. Schwerer, Lunar rock magnetism. *Moon* **4**, 170–196 (1972).
64. D. W. Collinson, S. K. Runcorn, A. Stephenson, A. J. Manson, Magnetic properties of Apollo 14 rocks and fines. *Proc. Lunar Planet. Sci. Conf.* **3**, 2343–2361 (1972).
65. M. Fuller, S. M. Cisowski, Lunar paleomagnetism, in *Geomagnetism*, J. A. Jacobs, Ed. (Academic Press, 1987), vol. 2, pp. 307–456.
66. P. Rochette, J. Gattacceca, A. V. Ivanov, M. A. Nazarov, N. S. Bezaeva, Magnetic properties of lunar materials: Meteorites, Luna and Apollo returned samples. *Earth Planet. Sci. Lett.* **292**, 383–391 (2010).
67. C. Cournéde, J. Gattacceca, P. Rochette, Magnetic study of large Apollo samples: Possible evidence for an ancient centered dipolar field on the Moon. *Earth Planet. Sci. Lett.* **331-332**, 31–42 (2012).
68. D. F. Weill, R. A. Grieve, I. S. McCallum, Y. Bottinga, Mineralogy-petrology of lunar samples. Microprobe studies of samples 12021 and 12022; viscosity of melts of selected lunar compositions. *Proc. Lunar Sci. Conf.* **2**, 413 (1971).
69. B. M. French, L. S. Walter, K. F. J. Heinrich, P. D. Loman, A. S. Doan, I. Adler, Composition of major and minor minerals in five Apollo 12 crystalline rocks, NASA SP-306 (NASA, Greenbelt, MD, 1972).
70. R. A. Cliff, C. Lee-Hu, G. W. Wetherill, Rb–Sr and U, Th–Pb measurements on Apollo 12 material. *Proc. Lunar Sci. Conf.* **2**, 1493–1502 (1971).
71. D. A. Papanastassiou, G. J. Wasserburg, Lunar chronology and evolution from Rb-Sr studies of Apollo 11 and 12 samples. *Earth Planet. Sci. Lett.* **11**, 37–62 (1971).
72. M. R. Dence, J. A. V. Douglas, A. G. Plant, R. J. Traill, Mineralogy and petrology of some Apollo 12 samples. *Proc. Lunar Sci. Conf.* **1**, 285–299 (1971).
73. W. S. Baldridge, D. W. Beaty, S. M. R. Hill, A. L. Albee, The petrology of the Apollo 12 pigeonite basalt suite. *Proc. Lunar Planet. Sci. Conf.* 141–179 (1979).
74. P. Horn, T. Kirsten, E. K. Jessberger, Are there a 12 mare basalts younger than 3.1 b.y. Unsuccessful search for a 12 mare basalts with crystallization ages below 3.1 b.y. *Meteoritics* **10**, 417 (1975).
75. P. E. Champness, A. C. Dunham, F. G. F. Gibb, H. N. Giles, W. S. MacKenzie, E. F. Stumpel, J. Zussman, Mineralogy and petrology of some Apollo 12 lunar samples. *Proc. Lunar Sci. Conf.* **1**, 359–376 (1971).
76. R. C. Newton, A. T. Anderson, J. V. Smith, Accumulation of olivine in rock 12040 and other basaltic fragments in the light of analysis and syntheses. *Proc. Lunar Sci. Conf.* **2**, 575 (1971).
77. W. Compston, H. Berry, M. J. Vernon, B. W. Chappell, M. J. Kay, Rubidium-strontium chronology and chemistry of lunar material from the Ocean of Storms. *Proc. Lunar Sci. Conf.* **2**, 1471–1485 (1971).
78. R. F. Dymek, A. L. Albee, A. A. Chodos, Comparative mineralogy and petrology of Apollo 17 mare basalts: Samples 70215, 71055, 74255, 75055, in *Proceedings of the 6th Lunar Science Conference* (SAO/NASA Astrophysics Data System, 1975), pp. 49–77.
79. F. Tera, D. A. Papanastassiou, G. J. Wasserburg, The lunar time scale and a summary of isotopic evidence for a terminal lunar cataclysm. *Proc. Lunar Planet. Sci. Conf.* **5**, 792 (1974).
80. A. P. Roberts, C. R. Pike, K. L. Verosub, First-order reversal curve diagrams: A new tool for characterizing the magnetic properties of natural samples. *J. Geophys. Res.* **105**, 28461–28475 (2000).
81. R. J. Harrison, J. M. Feinberg, FORCinel: An improved algorithm for calculating first-order reversal curve distributions using locally weighted regression smoothing. *Geochem. Geophys. Geosyst.* **9**, Q05016 (2008).
82. R. Egli, VARIFORC: An optimized protocol for calculating non-regular first-order reversal curve (FORC) diagrams. *Global Planet. Change* **110**, 302–320 (2013).
83. B. P. Weiss, S. M. Tikoo, The lunar dynamo. *Science* **346**, 1246753 (2014).
84. S. M. Tikoo, B. P. Weiss, J. Buz, E. A. Lima, E. K. Shea, G. Melo, T. L. Grove, Magnetic fidelity of lunar samples and implications for an ancient core dynamo. *Earth Planet. Sci. Lett.* **337-338**, 93–103 (2012).
85. A. Stephenson, D. Collinson, Lunar magnetic field palaeointensities determined by an anhysteretic remanent magnetization method. *Earth Planet. Sci. Lett.* **23**, 220–228 (1974).
86. S. M. Tikoo, B. P. Weiss, W. S. Cassata, D. L. Shuster, J. Gattacceca, E. A. Lima, C. Suavet, F. Nimmo, M. D. Fuller, Decline of the lunar core dynamo. *Earth Planet. Sci. Lett.* **404**, 89–97 (2014).
87. S. M. Tikoo, B. P. Weiss, J. Buz, I. Garrick-Bethell, T. L. Grove, J. Gattacceca, Ancient lunar dynamo: Absence of evidence is not the evidence of absence. *Lunar Planet. Sci. Conf.* **41**, 2705 (2010).
88. C. Meyer, *15498, Lunar Sample Compendium* (NASA, 2011).
89. J. M. Christie, D. T. Griggs, A. H. Heuer, G. L. Nord Jr., S. V. Radcliffe, J. S. Lally, R. M. Fisher, Electron petrography of Apollo 14 and 15 breccias and shock produced analogs. *Proc. Lunar Planet. Sci. Conf.* **1**, 365–382 (1973).
90. D. R. Uhlmann, L. C. Klein, Crystallization kinetics, viscous flow and thermal histories of lunar breccias 15286 and 15498. *Proc. Lunar Planet. Sci. Conf.* **2**, 2529–2541 (1976).
91. A. R. Duncan, M. K. Sher, Y. C. Abraham, A. J. Erlank, J. P. Willis, L. H. Ahrens, Interpretation of the compositional variability of Apollo 15 soils. *Proc. Lunar Planet. Sci. Conf.* **2**, 2309–2320 (1975).
92. W. A. Gose, D. W. Strangway, G. W. Pearce, A determination of the intensity of the ancient lunar magnetic field. *Moon* **7**, 196–201 (1973).
93. R. F. Dymek, A. L. Albee, A. A. Chodos, Comparative petrology of lunar cumulate rocks of possible primary origin: Dunite 72415, troctolite 76535, norite 78235, and anorthosite 62237. *Proc. Lunar Planet. Sci. Conf.* **1**, 301–341 (1975).
94. I. Garrick-Bethell, K. Miljković, H. Hiesinger, C. H. van der Bogert, M. Laneuville, D. L. Shuster, D. G. Korycansky, Troctolite 76535: A sample of the Moon's South Pole-Aitken basin? *Icarus* **338**, 113430 (2020).
95. I. Garrick-Bethell, B. P. Weiss, D. L. Shuster, S. M. Tikoo, M. M. Tremblay, Further evidence for early lunar magnetism from troctolite 76535. *J. Geophys. Res.* **122**, 76–93 (2017).
96. H. Oda, J. Kawai, M. Miyamoto, I. Miyagi, M. Sato, A. Noguchi, Y. Yamamoto, J.-I. Fujihira, N. Natsuhara, Y. Aramaki, T. Masuda, C. Xuan, Scanning SQUID microscope system for geological samples: System integration and initial evaluation. *Earth Planets Space* **68**, 179 (2016).
97. J. A. Tarduno, R. D. Cottrell, R. K. Bono, H. Oda, W. J. Davis, M. Fayek, O. van 't Erve, F. Nimmo, W. Huang, E. Thern, S. Fearn, G. Mitra, A. V. Smirnov, E. G. Blackman, Paleomagnetism indicates that primary magnetite in zircon records a strong Hadean geodynamo. *Proc Natl. Acad. Sci. U.S.A.* **117**, 2309–2319 (2020).
98. J. A. Tarduno, R. D. Cottrell, F. Nimmo, J. Hopkins, J. Voronov, A. Erickson, E. Blackman, E. R. D. Scott, R. McKinley, Evidence for a dynamo in the main group pallasite parent body. *Science* **338**, 939–942 (2012).
99. R. D. Cottrell, J. A. Tarduno, In search of high-fidelity geomagnetic paleointensities: A comparison of single plagioclase crystal and whole rock Thellier-Thellier analyses. *J. Geophys. Res.* **105**, 23579–23594 (2000).
100. J. Gattacceca, P. Rochette, Toward a robust normalized magnetic paleointensity method applied to meteorites. *Earth Planet. Sci. Lett.* **227**, 377–393 (2004).
101. D. R. Finn, R. S. Coe, A new protocol for three-axis static alternating field demagnetization of rocks. *Geochem. Geophys. Geosyst.* **17**, 1815–1822 (2016).
102. G. Kletetschka, T. Kohout, P. Wasilewski, Magnetic remanence in the Murchison meteorite. *Meteorit. Planet. Sci.* **38**, 399–405 (2003).
103. G. Kletetschka, M. A. Wieczorek, Fundamental relations of mineral specific magnetic carriers for paleointensity determination. *Phys. Earth Planet. Inter.* **272**, 44–49 (2017).
104. G. S. Collins, H. J. Melosh, B. A. Ivanov, Modeling damage and deformation in impact simulations. *Meteorit. Planet. Sci.* **39**, 217–231 (2004).
105. K. Wünnemann, G. S. Collins, H. J. Melosh, A strain-based porosity model for use in hydrocode simulations of impacts and implications for transient crater growth in porous targets. *Icarus* **180**, 514–527 (2006).
106. D. A. Crawford, P. H. Schultz, Laboratory observations of impact-generated magnetic fields. *Nature* **336**, 50–52 (1988).
107. D. A. Crawford, P. H. Schultz, Electromagnetic properties of impact-generated plasma, vapor and debris. *Int. J. Impact Eng.* **23**, 169–180 (1999).
108. L. Carporzen, B. P. Weiss, S. A. Gilder, A. Pommier, R. J. Hart, Lightning remagnetization of the Vredefort impact crater: No evidence for impact-generated magnetic fields. *J. Geophys. Res.* **117**, E01007 (2012).

109. S. A. Gilder, J. Pohl, M. Eitel, Magnetic signatures of terrestrial meteorite impact craters: A summary, in *Magnetic Fields in the Solar System*, H. Luhr, J. Wicht, S. A. Gilder, M. Holschneider, Eds. (Springer, 2018), pp. 357–382.
110. K. L. Louzada, B. P. Weiss, A. C. Maloof, S. T. Stewart, N. L. Swanson-Hysell, S. Adam Soule, Paleomagnetism of Lonar impact crater, India. *Earth Planet. Sci. Lett.* **275**, 308–319 (2008).
111. B. P. Weiss, S. Pedersen, I. Garrick-Bethell, S. T. Stewart, K. L. Louzada, A. C. Maloof, N. L. Swanson-Hysell, Paleomagnetism of impact spherules from Lonar crater, India and a test for impact-generated fields. *Earth Planet. Sci. Lett.* **298**, 66–76 (2010).
112. F. Jourdan, F. Moynier, C. Koeberl, 40Ar/39Ar age of the Lonar crater and consequence for the geochronology of planetary impacts. *Geology* **39**, 671–674 (2011).
113. S. J. Robbins, A new global database of lunar impact craters >1-2 km: 1. Crater locations and sizes, comparisons with published databases, and global analysis. *J. Geophys. Res.* **124**, 871–892 (2018).
114. C. Yang, H. Zhao, L. Bruzzone, J. A. Benediktsson, Y. Liang, B. Liu, X. Zeng, R. Guan, C. Li, Z. Ouyang, Lunar impact crater identification and age estimation with Chang'E data by deep and transfer learning. *Nat. Commun.* **11**, 6358 (2020).
115. G. Neukum, B. A. Ivanov, W. K. Hartmann, Cratering records in the inner solar system in relation to the lunar reference system. *Space Sci. Rev.* **96**, 55–86 (2001).
116. D. Stöffler, G. Ryder, Stratigraphy and isotope ages of lunar geologic units: Chronological standard for the inner Solar System. *Space Sci. Rev.* **96**, 9–54 (2001).
117. C. M. Fortezzo, P. D. Spudis, S. L. Harrel, Release of the digital unified global geologic map of the Moon at 1:5,000,000- Scale, paper presented at the 51st Lunar and Planetary Science Conference, Lunar and Planetary Institute, Houston, TX, 3 March 2020.
118. M. E. Purucker, J. B. Nicholas, Global spherical harmonic models of the internal magnetic field of the Moon based on sequential and coestimation approaches. *J. Geophys. Res.* **115**, E12007 (2010).
119. R. Day, M. Fuller, V. A. Schmidt, Hysteresis properties of titanomagnetites: Grain-size and compositional dependence. *Phys. Earth Planet. Inter.* **13**, 260–267 (1977).
120. D. J. Dunlop, Theory and application of the Day plot (M_{rs}/M_s versus H_{cr}/H_c) 1. Theoretical curves and tests using titanomagnetite data. *J. Geophys. Res.* **107**, EPM 4-1–EPM 4-22 (2002).
121. P. Wasilewski, Magnetization of small iron–nickel spheres. *Phys. Earth Planet. Inter.* **26**, 149–161 (1981).
122. R. S. Coe, The determination of paleo-intensities of the Earth's magnetic field with emphasis on mechanisms which could cause non-ideal behavior in Thellier's method. *J. Geomag. Geoelec.* **19**, 157–179 (1967).
123. P. A. Selkin, L. Tauxe, Long-term variations in palaeointensity. *Phil. Trans. R. Soc. A* **358**, 1065–1088 (2000).
124. C. Suavet, B. P. Weiss, W. S. Cassata, D. L. Shuster, J. Gattacceca, L. Chan, I. Garrick-Bethell, J. W. Head, T. L. Grove, M. D. Fuller, Persistence and origin of the lunar core dynamo. *Proc. Natl. Acad. Sci. U.S.A.* **110**, 8453–8458 (2013).

Acknowledgments: We thank G. Kloc for assistance in sample preparation and B.L. McIntyre on electron microscopy analyses. We greatly appreciate helpful reviews from D. Dunlop and two anonymous reviewers. **Funding:** This work was supported by NSF grants EAR1656348 (to J.A.T.) and PHY-2020249 (E.G.B. and M.N.), NASA grants 80NSSC19K0510 (to J.A.T.) and PGG-NNX13AO33G (to C.L.J. and K.L.), and a JSPS fellowship (to J.A.T.). **Author contributions:** K.L. selected samples for analysis. R.D.C. and K.L. performed remanence and rock magnetic measurements. R.K.B., W.H., T.Z., and B.C. conducted SEM analyses. Experimental data were analyzed by these authors together with J.A.T. and A.V.S. H.O. contributed measurements on materials. M.N. performed numerical impact modeling. E.G.B. contributed impact theory. C.R.N. and M. I.-M. provided petrologic and age context. C.L.J. and K.L. conceived the initial study. J.A.T. designed and supervised subsequent investigations. J.A.T. wrote the manuscript with input from all the authors. **Competing interests:** The authors declare that they have no competing interests. **Data and materials availability:** All data needed to evaluate the conclusions in the paper are present in the paper and/or the Supplementary Materials. Requests for Apollo lunar samples for study are directed to NASA (https://curator.jsc.nasa.gov/lunar/sampreq). Data presented here are available in the EarthRef (MagIC) database (earthref.org/MagIC/17143). Additional data related to this paper may be requested from the authors.

Submitted 29 March 2021
Accepted 16 June 2021
Published 4 August 2021
10.1126/sciadv.abi7647

Citation: J. A. Tarduno, R. D. Cottrell, K. Lawrence, R. K. Bono, W. Huang, C. L. Johnson, E. G. Blackman, A. V. Smirnov, M. Nakajima, C. R. Neal, T. Zhou, M. Ibanez-Mejia, H. Oda, B. Crummins, Absence of a long-lived lunar paleomagnetosphere. *Sci. Adv.* **7**, eabi7647 (2021).

Science Advances

Absence of a long-lived lunar paleomagnetosphere

John A. Tarduno, Rory D. Cottrell, Kristin Lawrence, Richard K. Bono, Wentao Huang, Catherine L. Johnson, Eric G. Blackman, Aleksey V. Smirnov, Miki Nakajima, Clive R. Neal, Tinghong Zhou, Mauricio Ibanez-Mejia, Hirokuni Oda and Ben Crummins

Sci Adv **7** (32), eabi7647.
DOI: 10.1126/sciadv.abi7647